Low-temperature Wollastonite Formed by Carbonate Reduction: a Marker of Serpentinite Redox Conditions

BENJAMIN MALVOISIN[1,2]*, CHRISTIAN CHOPIN[1], FABRICE BRUNET[1,2] AND MATTHIEU E. GALVEZ[3]

[1]LABORATOIRE DE GÉOLOGIE, ECOLE NORMALE SUPÉRIEURE–CNRS, 24 RUE LHOMOND, 75231 PARIS CEDEX 5, FRANCE

[2]ISTERRE, CNRS–UNIVERSITÉ JOSEPH FOURIER, MAISON DES GÉOSCIENCES, BOÎTE POSTE 53, 38041 GRENOBLE CEDEX 9, FRANCE

[3]IMPMC, CAMPUS JUSSIEU, BOÎTE COURRIER 115, 4, PLACE JUSSIEU, 75252 PARIS CEDEX 05, FRANCE

In the Alpine blueschist- to eclogite-facies meta-ophiolitic units of northern Corsica, the contact between a serpentinite body and an immediately overlying siliceous marble is remarkable for the occurrence of wollastonite and, on the marble side, a dark halo around the serpentinite. The refolded, continuous contact is a rodingite-type reaction zone with a centimetre-thick nephritic selvage of diopside + andradite/grossular ± perovskite on the serpentinite side, followed towards the marble by a 1–5 cm thick zone of massive wollastonite (± grossular), followed by a 5–20 cm thick dark zone (the halo) consisting of wollastonite + quartz + graphitic material (± grossular ± diopside), with no carbonate. The transition to the overlying wollastonite-free, calcite + quartz-bearing layers is sharp. Considering the stability of calcite + quartz everywhere else in the regional metamorphic series, this low-temperature occurrence of wollastonite (c. 400–450°C) requires unusual conditions. A clue to its origin is the abundance of graphitic matter with the wollastonite within a few decimetres of the serpentinite body. We interpret this observation as evidence for local reduction of Ca-carbonate to form elemental carbon and wollastonite according to the reaction

$$SiO_2 + CaCO_3 + 2\,H_2 \rightarrow CaSiO_3 + C + 2\,H_2O.$$

A similar carbonate + mica reduction reaction is responsible for the disappearance of phengite and the appearance of grossular + carbon within a narrow zone in the marble above the wollastonite–quartz zone. Textural and solubility considerations suggest that the development of the zonal sequence is an essentially diffusive process. Thermochemical modelling of mineral stability in the successive reaction zones suggests a positive oxygen-fugacity gradient from the serpentinite to the marble ($-6 < \Delta FMQ < -1$), mediated through a CH_4- and H_2-bearing aqueous intergranular fluid. In line with the field evidence, it is calculated that a serpentinite body equilibrated at ΔFMQ -4 after oceanic serpentinization can still impose, through Fe^{2+}-bearing serpentine oxidation, highly reducing conditions while entrained at depth in a subduction wedge and channel. This may contribute to the presence of $H_2 \pm CH_4$ in the fluid and cause the destabilization of calcite in favour of graphite. In addition to the consequences for wollastonite and elemental carbon formation at low temperature, this finding has direct implications for redox conditions in subduction zones.

KEY WORDS: *wollastonite; redox; serpentinite; carbonate reduction; H_2 and CH_4 fluids; rodingite; blueschist; Corsica*

INTRODUCTION

Hydrothermal interaction between seawater and oceanic peridotite leads to the formation of hydrous phases dominated by serpentine-group minerals. The progressive transformation of nominally anhydrous peridotite to

*Corresponding author. Present address: ISTerre, Maison des Géosciences Boîte Poste 53, 38041 Grenoble cedex 9, France. E-mail: benjamin.malvoisin@ujf-grenoble.fr

serpentinite (serpentinization) not only affects the bulk water content of the rock system but it also strongly modifies its redox potential. Peridotite–seawater interaction results in the oxidation of Fe in the original ultramafic rock and in the corresponding reduction of the aqueous fluid that may, ultimately, dissociate to form H_2 (Moody, 1976; Charlou, 2002; Kelley et al., 2005). Hydrated peridotites are incorporated into subduction zones (Rüpke et al., 2004; Iyer et al., 2010) where they can interact chemically with the mantle wedge, in particular when they start dehydrating (Deschamps et al., 2010). Obviously, the redox potential of this released fluid will depend on the oxidation state of the parent serpentinite. As an insight into the redox conditions associated with serpentinite environments, we report here petrological evidence for the development of a reduced halo in marble in contact with a serpentinite body that experienced blueschist- to eclogite-facies metamorphic conditions as part of an Alpine ophiolite complex in Corsica. We show that serpentinite may preserve and locally impose some of its initial redox conditions throughout the vagaries of subduction and exhumation.

The incentive for this study was the discovery of wollastonite, nominally a high-temperature mineral, in low-temperature, blueschist- to eclogite-facies rocks from Corsica. This paradoxical occurrence is strictly bound to a zone of graphitic-matter enrichment along a serpentinite–marble interface. It is completely at odds with the classical regional- or contact-metamorphic origin of wollastonite through high-temperature devolatilization of a calcite–quartz assemblage (e.g. Trommsdorff, 1968; Ferry et al., 2001). The stability of calcite + quartz throughout the Alpine low-T metamorphic pile in Corsica calls for another origin for the wollastonite. We show that its occurrence in Corsica along with graphitic matter is the result of the reduction of carbonate around the serpentinite body during metamorphism. This provides evidence for the maintenance of the reducing potential of serpentinites during subduction and accretionary-wedge evolution.

GEOLOGICAL SETTING

The northeastern part of Corsica belongs to the Alpine orogen (Fig. 1, inset) and consists mainly of Mesozoic formations of oceanic derivation, some of them possibly transitional between a continental margin (to the west) and more typical ophiolitic units (e.g. Faure & Malavieille, 1981; Jolivet et al., 1990; Malavieille et al., 1998; Vitale Brovarone et al., 2011a, for more details). Most units were buried and metamorphosed under high-pressure and low-temperature conditions during the Alpine orogeny; some reached the lawsonite-eclogite facies (Caron & Péquignot, 1986; Ravna et al., 2010; Vitale Brovarone et al., 2011b). At Cap Corse, the northern tip of the island (Fig. 1), the metamorphic pile comprises several ophiolitic

units, mostly serpentinite with some gabbro, basalt, peridotite and subordinate sedimentary material including radiolarite and calcschist. Other intercalated units comprise material of more continental derivation (e.g. the Farinole and Serra di Pigno gneisses). The metamorphic grade may not be uniform throughout the pile. The Farinole series contains jadeite-bearing metagranite and lawsonite-eclogite, for which early estimates by Lahondère (1988) were $P > 1$ GPa, T(grt–cpx inclusion) ~ 430–$520°$C, T(grt–cpx in matrix) ~ 500–$600°$C, revised to $P > 1.5$ GPa, $T \sim 450$–$490°$C if one combines Lahondère's (1996) new estimates for orthogneiss and metabasite [mineral names are abbreviated after Kretz (1983), capitalized for end-members; e.g. Aeg for aegirine]. More recent estimates for lawsonite-eclogite in meta-pillow-basalts of the Lancône Pass, a structurally deeper unit about 10 km further south, are 1.9–2.6 GPa, 340–415°C (Ravna et al., 2010), revised to 2.3 ± 0.1 GPa and $520 \pm 20°$C by Vitale Brovarone et al. (2011b). In the structurally higher, blueschist-facies ophiolitic units exposed along the Cap Corse ridge, temperatures did not exceed 350–430°C as indicated by relics of Fe–Mg-carpholite and thermometry based on Raman spectroscopy of carbonaceous material (RSCM thermometry, Vitale Brovarone et al., in preparation). The following description pertains to one of them.

Above the village of Patrimonio, the Malaspina ridge, which leads to the Serra di Pigno, exposes slivers of a metasedimentary series within a large serpentinite body (which overlies the Farinole–Serra di Pigno gneisses, which themselves lie structurally above meta-ophiolitic units of the Lancône Pass; Fig. 1). The largest sliver, less than 100 m across strike, consists of massive beds of siliceous marble with carbonate-bearing quartzite at its base, grading upwards into more pelitic layers with a few mafic intercalations. The series rests in direct contact with the serpentinite and was refolded with it, as shown by metre-scale recumbent and sheath folds affecting the contact that are well exposed on the ridge and on its northern side at about 480 m elevation. The marble–serpentinite contact is generally concordant with the sedimentary bedding, as far as one can judge from lithological heterogeneities. This sedimentary series may represent the stratigraphic cover of a tectonized ocean floor (but see Vitale Brovarone et al., 2011a).

Minerals found in the first few metres of the series above the serpentinite (i.e. in the more carbonate-rich layers) are calcite, quartz, clinozoisite, titanite, apatite, graphitic material, rare phengite, albite, and locally prehnite. Aragonite (Chopin et al., 2008) occurs exclusively as oriented fibres in garnet crystals within a black calcite marble layer that immediately overlies the serpentinite (see below), and to which garnet is restricted, along with minor diopside. Glaucophane ('crossite') and phengite occur in the more pelitic layers, higher in the series.
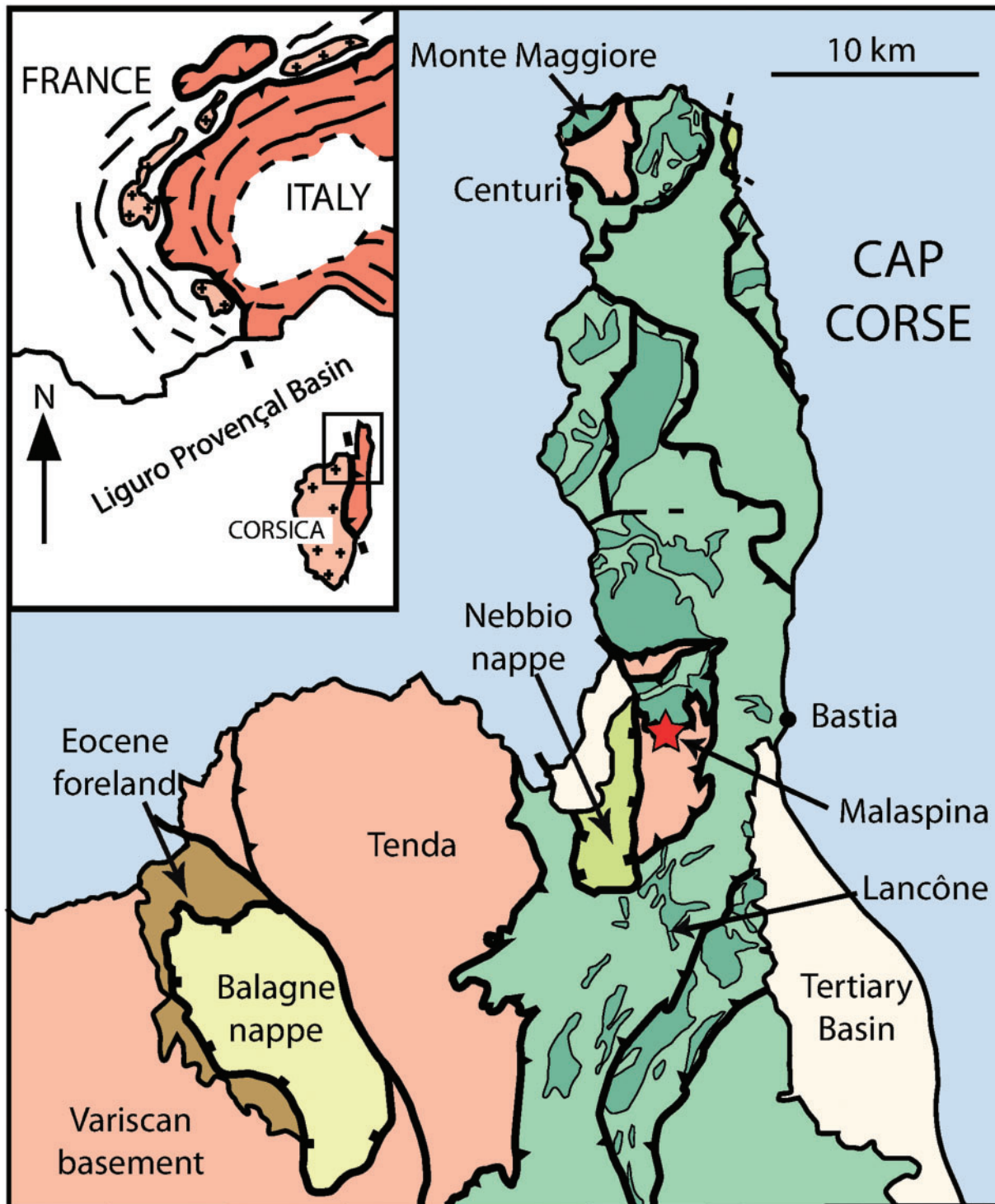
Fig. 1. Geological sketch map of the Cap Corse area, NE Corsica, after Malavieille *et al.* (1998) and Chopin *et al.* (2008). Flesh colour refers to continental units (Variscan basement) with parautochthonous cover (brown), green refers to the metamorphic oceanic units with a darker shade for serpentinite bodies, greenish yellow to the uppermost, nearly non-metamorphic nappes. The star indicates the location of the Cima di Malaspina outcrop. Inset: Alpine chain with internal units (reddish brown) and external crystalline massifs (flesh colour).
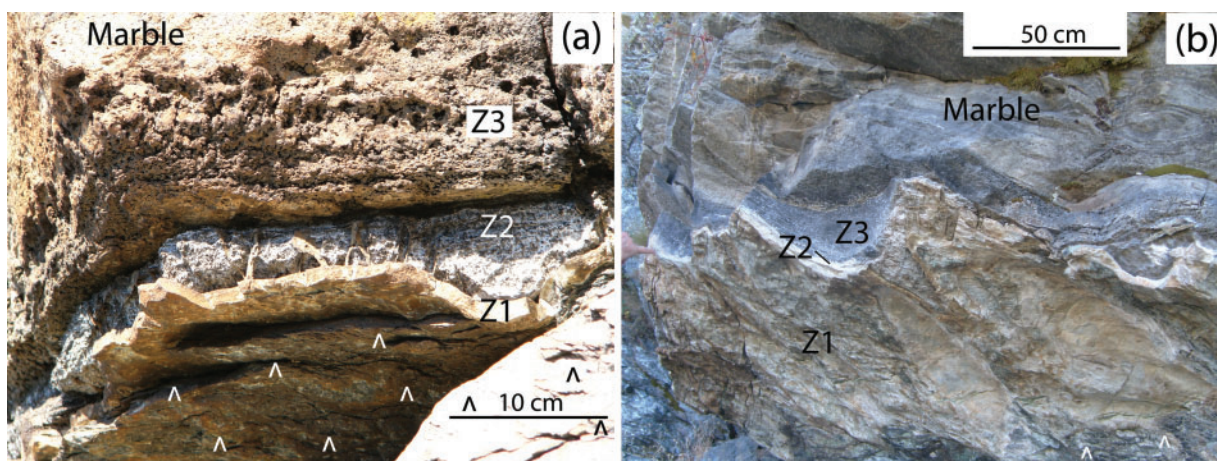
Fig. 2. Field photographs of the reaction zone between serpentinite (∧) and marble. (a) On the weathered outcrop, alteration reveals the layered structure of the reaction zone with, from deformed serpentinite to marble, a very tough, protruding yellowish zone (Z1), a more alterable grey zone (Z2), and a zone similar in texture to the overlying marble but displaying weathering pits (Z3). Photograph courtesy of O. Beyssac. (b) Fresh cut of the gently folded reaction zone showing the same zonation as in (a). The Z1 and Z2 layers, each about 1 cm thick, form an overhang above the serpentinite; the darker colour of the Z3 layer should be noted.

THE SERPENTINITE–MARBLE INTERFACE

At the Malaspina outcrop, the serpentinite–marble contact (Fig. 2) is marked by a centimetre-thick, weathering-resistant rim of calc-silicate rock, which is remarkable for its continuity throughout the outcrop (i.e. over about 100 m), regardless of the folded nature of the contact (see Fig. S1 in the Supplementary Material, which is available for downloading at http://www.petrology.oxfordjournals/org), suggesting a syn- to post-folding formation. As such this kind of contact is a classical geological feature, long recognized as a reaction zone between serpentinite and country-rock [= 'skarn', 'rodingite' or 'nephrite'; see Coleman (1967) and Harlow *et al.* (2007) for a review]. However, this contact shows two unusual features: one is the occurrence of wollastonite, and the other is the presence of a conspicuous dark halo, typically one to a few decimetres thick, in the marble directly overlying the contact (Fig. 2). The dark colour is due to the presence of graphitic matter, which is locally so abundant as to stain the fingers.

Differential weathering outlines the fine structure of the reaction zone (Fig. 2a) and reveals, from the serpentinite to the marble, three layers of distinctive colour: a protruding, very resistant, whitish nephritic layer, 0·5–3 cm thick (zone Z1); a massive but less resistant pale greyish zone ranging from 0·5 to 5 cm in thickness (zone Z2); and a darker, 5–25 cm thick zone that preserves the appearance and original texture of the marble except for numerous weathering pits (zone Z3, Fig. 2a). A fresher cut across this contact (Fig. 2b) and detailed observation of samples confirm the three sharp zones and highlight the darkness of zone Z3.

ANALYSIS OF THE REACTION ZONE

Analytical methods

The mineral content of the various contact zones has been characterized from a series of thin sections using optical microscopy. Mineral compositions were obtained by electron microprobe analyses (SX100 Cameca instrument at Camparis, UPMC, Paris, in wavelength-dispersive mode, 15 kV, 15 nA, with mineral standards and PAP correction). Further chemical (elemental X-ray mapping) and textural data [back-scattered electron (BSE) images] were obtained using an FE-SEM (Zeiss–Σigma^{TM}) equipped with a 50 mm^2 EDS detector (X-Max^{TM}, Oxford Instruments) at the Ecole normale supérieure (ENS, Paris). The EDS detector can quantify concentrations of more than 1 mol % with an accuracy of 5% and qualitatively detects elements reaching concentrations of more than 0·1 mol %. Raman microspectometry was used to determine the mineralogy of serpentine using a Renishaw inVia spectrometer at ENS with a 514·5 nm argon laser focused through a DMLM Leica optical microscope. The mineral modes in the reaction zone were determined from both BSE images and X-ray maps. The composition (point analysis) and the associated colour range were first determined for each mineral. Then, mineral identification was performed automatically by correlating the BSE images and X-ray maps for each pixel of 3 μm. Finally, the surface area of each mineral (interpreted as the mineral mode) across the reaction zone was determined in the form of a reconstituted profile with 30 images pasted together. Total organic content (TOC) measurements were performed on ∼1 cm^3 samples drilled from the reaction zone, by combustion under oxygen at 1400°C with a

Table 1: Garnet and clinopyroxene composition in serpentine and the reaction zones

	Garnet								Clinopyroxene					
Sample:	09-10	09-10	09-04	09-05	09-04	09-04	09-04		10-10	10-10	09-11	09-04	09-05	09-05
Zone:	Serp	Serp	Z1	Z1	Z1/Z2	Z2	Z3		Serp	Serp	Serp	Z1	Z1	Z2
SiO_2	34·93	35·34	35·78	36·57	37·43	37·53	39·27	SiO_2	52·83	54·05	54·94	55·89	55·01	54·34
TiO_2	0·75	0·67	0·03	0·02	0·56	0·07	0·40	TiO_2	0·23	0·14	0·03	0·02	0·00	0·00
Al_2O_3	0·39	1·37	1·32	2·30	9·81	8·25	21·38	Al_2O_3	3·45	1·33	0·05	0·00	0·03	0·33
Cr_2O_3	18·09	14·20	0·01	0·00	0·02	0·00	0·00	Cr_2O_3	0·75	0·20	0·00	0·00	0·00	0·00
Fe_2O_3	12·14	13·78	28·86	27·15	17·04	19·08	1·24	FeO	2·62	2·09	0·68	0·51	1·03	3·69
MnO	0·00	0·00	0·12	0·09	0·23	0·12	0·48	MnO	0·06	0·12	0·11	0·12	1·30	2·16
MgO	0·06	0·11	0·00	0·00	0·00	0·00	0·00	MgO	16·69	17·78	18·56	17·69	16·98	14·23
CaO	33·44	34·08	33·44	33·62	35·10	34·98	36·77	CaO	22·70	23·54	25·40	26·23	25·84	25·43
Na_2O	0·04	0·02	0·00	0·01	0·04	0·08	0·00	Na_2O	0·53	0·27	0·04	0·02	0·00	0·07
NiO	0·00	0·06	0·02	0·00	0·00	0·00	0·00	NiO	0·00	0·00	0·00	0·00	0·02	0·00
Total	99·85	100·02	99·60	99·83	100·36	100·25	100·03	Total	99·93	99·56	99·88	100·59	100·56	100·28
	Structural formula based on 8 cations								Structural formula based on 4 cations					
Si	2·929	2·950	3·011	3·052	2·990	3·019	2·976	Si	1·919	1·966	1·986	2·015	2·000	2·008
Ti	0·047	0·042	0·002	0·001	0·033	0·004	0·023	Ti	0·006	0·004	0·001	0·000	0·000	0·000
Al	0·039	0·135	0·131	0·226	0·923	0·782	1·910	Al	0·148	0·057	0·002	0·000	0·001	0·014
Cr	1·199	0·937	0·000	0·000	0·001	0·000	0·000	Cr	0·022	0·006	0·000	0·000	0·000	0·000
Fe^{3+}	0·767	0·867	1·830	1·707	1·026	1·156	0·071	Fe	0·080	0·064	0·020	0·015	0·031	0·114
Fe^{2+}	0·000	0·000	0·000	0·000	0·000	0·000	0·000	Mn	0·002	0·004	0·003	0·004	0·040	0·067
Mn	0·000	0·000	0·008	0·007	0·016	0·008	0·031	Mg	0·904	0·964	1·000	0·951	0·920	0·784
Mg	0·007	0·013	0·000	0·000	0·000	0·000	0·000	Ca	0·883	0·917	0·984	1·013	1·007	1·007
Ca	3·004	3·048	3·016	3·006	3·004	3·015	2·986	Na	0·037	0·019	0·003	0·001	0·000	0·005
Na	0·006	0·004	0·000	0·001	0·007	0·013	0·000	Ni	0·000	0·000	0·000	0·000	0·001	0·000
Ni	0·000	0·004	0·001	0·000	0·000	0·000	0·000							
Almandine %	0·00	0·00	0·00	0·00	0·00	0·00	0·00	Mg#	0·92	0·94	0·98	0·98	0·97	0·87
Andradite %	39·01	45·90	93·30	88·30	52·87	59·67	3·62							
Grossular %	0·00	4·46	6·65	11·66	46·76	40·19	95·37							
Pyrope %	0·00	0·02	0·00	0·00	0·00	0·00	0·00							
Spessartine %	0·00	0·00	0·03	0·04	0·31	0·14	1·01							
Uvarovite %	60·99	49·62	0·02	0·00	0·05	0·00	0·00							

Carbon–Nitrogen LECO SC l44DRPC analyser at the Service d'Analyse des Roches et des Minéraux (CRPG, Vandoeuvre-lès-Nancy).

Petrography and mineral chemistry
Serpentinite
The serpentinite shows a pronounced schistosity (Fig. 2a). Samples collected within 1 m of the contact are mainly composed of serpentine, Cr–Fe oxides, clinopyroxene and uvarovite-rich garnet (Tables 1 and 2), as are those collected further away. Neither orthopyroxene, olivine, brucite, a humite-group mineral, nor Fe–Ni alloys were found here.

Serpentine occurs as platy crystals. It displays three Raman peaks at 1045, 3665 and 3697 cm^{-1}, which are attributed to the antigorite polymorph (Lemaire *et al.*, 1999; Auzende *et al.*, 2004). Serpentine composition (Table 2) shows significant Al_2O_3 content variations at the thin-section scale, between 1·5 and 6·5 wt % (i.e. variable amesite component) and Mg/(Fe + Mg + Mn) varying from 0·90 to 0·97. Serpentine of similar composition (Table 2) is also found in thin veinlets penetrating the

Table 2: Serpentine, chlorite, balangeroite, wollastonite, carbonate, mica and talc composition in serpentinite and the reaction zones

	Serpentine				Chlorite	'Balangeroite'	Wollastonite	Carbonate			Phengite		Talc
Sample:	09-11	10-10	09-10	09-04	09-10	MAL	09-04	09-04			09-04	09-05	09-04
Zone:	Serp	Serp	Serp	Serp/Z1	Serp	Serp	Z3	Marble			Marble	Marble	Marble
SiO_2	41·16	42·94	41·33	39·16	31·87	19·83	51·62	0·02	SiO_2		53·43	52·33	51·65
TiO_2	0·01	0·01	0·00	0·03	0·06	0·02	0·02	0·04	TiO_2		0·13	0·02	0·03
Al_2O_3	2·97	1·60	2·20	3·35	6·98	0·34	0·01	0·01	Al_2O_3		19·57	24·50	0·64
FeO	2·91	2·62	2·41	3·50	3·76	47·68	0·02	0·00	FeO		3·02	3·11	0·42
MnO	0·08	0·24	0·12	0·30	0·00	0·00	0·00	0·00	MnO		0·30	0·04	0·27
MgO	38·38	39·06	39.·21	39·05	34·36	3·28	0·00	0·00	MgO		4·85	3·20	27·19
CaO	0·04	0·07	0·04	0·15	0·08	0·57	47·82	58·70	CaO		0·37	0·02	0·29
Cr_2O_3	0·22	0·42	0·20	0·02	10·06	0·05	0·07	0·00	Na_2O		0·00	0·01	0·04
NiO	0·24	0·14	0·38	0·06	0·00	13·39	0·00	0·12	K_2O		10·67	10·61	0·30
Total	86·00	87·19	86·04	86·02	87·18	85·26	99·76	59·00	Cr_2O_3		0·02	0·05	0·00
									NiO		0·25	0·14	0·07
									Total		92·98	94·34	81·18

Structural formula

based on:	7(O)	7(O)	7(O)	7(O)	14(O)	58 cations	2 cations	1 cation			11(O)	11(O)	11(O)
Si	1·949	2·003	1·958	1·879	3·140	15·019	1·002	0·000	Si		3·694	3·545	3·886
Ti	0·000	0·000	0·000	0·001	0·002	0·010	0·000	0·000	Ti		0·007	0·001	0·002
Al	0·166	0·088	0·123	0·189	0·800	0·299	0·000	0·000	Al		1·595	1·957	0·056
Fe	0·115	0·102	0·095	0·141	0·300	30·198	0·000	0·000	Fe		0·175	0·176	0·027
Mn	0·003	0·009	0·005	0·012	0·000	0·000	0·000	0·000	Mn		0·017	0·003	0·017
Mg	2·710	2·716	2·770	2·793	5·040	3·700	0·000	0·000	Mg		0·500	0·323	3·050
Ca	0·002	0·003	0·002	0·008	0·004	0·466	0·995	0·997	Ca		0·028	0·001	0·023
Cr	0·008	0·015	0·007	0·001	0·780	0·032	0·001	0·000	Na		0·000	0·001	0·006
Ni	0·009	0·005	0·015	0·002	0·000	8·159	0·000	0·002	K		0·941	0·917	0·029
Mg#	0·96	0·96	0·97	0·95	0·94				Cr		0·001	0·003	0·000
									Ni		0·001	0·003	
									Celadonite %		66·18	46·94	
									Muscovite %		27·47	43·77	
									Paragonite %		0·00	0·12	
									Pyrophyllite %		5·24	8·02	

contact zone until zone Z2 but with a more prismatic morphology, which is probably related to a later generation. Small anhedral clinopyroxene crystals (5–20 µm across) are concentrated in planes parallel to the schistosity. Clinopyroxenes have high CaO contents (22·7–26·1 wt %) and low Al_2O_3 (0–3·5 wt %) and FeO_{tot} contents (0·7–2·7 wt %) corresponding to Mg/(Mg + Fe) ratios of 0·92–0·98 (Table 1). The analysis of SEM images

(about 1 mm^2) reveals that magnetite occupies between 0·1 and 11% of the image surface. Garnet (up to 100 µm in size, 55 mol % uvarovite–45 mol % andradite, Table 1), associated with Cr-bearing magnetite (up to 23 wt % Cr_2O_3) and some chlorite (up to 10 wt % Cr_2O_3, Table 2), forms small aggregates in the serpentinite (Fig. 3), most probably on the site of former Cr-rich spinel. In two samples, a reddish and elongated silicate mineral (aggregates
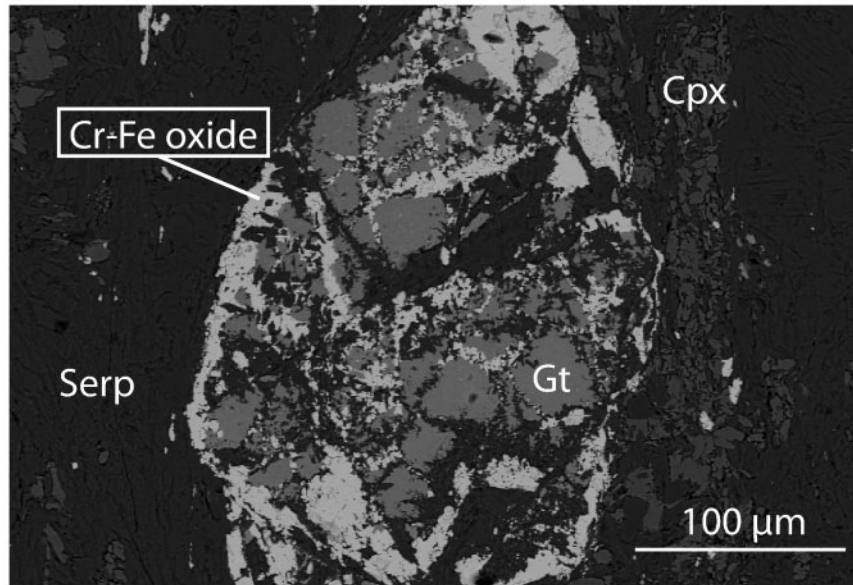
Fig. 3. Back-scattered electron (BSE) image of serpentinite showing a garnet + Cr–Fe oxide ± chlorite aggregate and clinopyroxene in the serpentine foliation (sample 10-10), suggesting garnet formation from former chromite and clinopyroxene.

of up to 100 µm across) was found intercalated with serpentine, with high FeO_{tot} (47·7–51·1 wt %) and NiO (4·3–13·4 wt %) contents and a low SiO_2 content of 15·2–19·8 wt % (Table 2). Its stoichiometry matches that of balangeroite, $Mg_{42}Si_{16}O_{54}(OH)_{40}$ (Compagnoni *et al.*, 1983) with Fe and Ni substituting for Mg. Similar Fe- and Ni-rich balangeroite was recently described by Evans & Kuehner (2011) in a serpentinite from Japan. A few small grains (less than 5 µm in size) of both ilmenite and pentlandite with up to 3 mol % of Co_9S_8 were also found. A few grains of native copper were observed in the serpentinite immediately underlying zone Z1.

Marble

The marble bed overlying the serpentinite is composed of varying proportions of calcite and quartz (*c.* 100 µm grain size), reflecting the original sedimentary compositional layering (Fig. 4a, bottom; Fig. 5d). It contains minor amounts of sheet-silicates, oriented parallel to the layering and the contact; these are a highly silicic phengitic mica with 3·5–3·7 Si per formula unit, sometimes interleaved or associated with a magnesian phase. This phase has a talc stoichiometry but low analytical totals suggestive of sepiolite (Table 1). Accessory phases are garnet, apatite, titanite and iron sulphide. A sample from which aragonite–garnet intergrowths have been described was found in an equivalent position (Chopin *et al.*, 2008).

Zone Z1

Zone Z1 is composed of extremely fine-grained clinopyroxene and garnet (Fig. 5a), hence its toughness, with accessory perovskite ($CaTiO_3$). The composition of garnet (typically 10–20 µm, up to 50 µm in size) lies on the andradite–grossular join (Table 1). The $X_{Fe^{3+}}$ ratio in the garnet octahedral site, defined as $X_{Fe^{3+}} = Fe^{3+}/(Al^{3+} + Fe^{3+})$, decreases from 0·98 in crystals close to the contact with the serpentinite to 0·4 in the vicinity of the next zone (Z2). BSE images show that the garnet is zoned, particularly close to zone Z2, with cores having lower $X_{Fe^{3+}}$ than rims. Clinopyroxene is close to the diopside end-member: $Ca(Mg_{1-x},Fe_x)Si_2O_6$ with *x* between 0·02 and 0·07. Late calcite veins locally cross-cut the serpentinite and zone Z1. Isolated tiny grains of native copper also occur in this zone.

Zone Z2

This zone is made almost completely of wollastonite, which is responsible for its easier weathering (Fig. 2), with subordinate garnet throughout and some diopside on the Z1 side (Fig. 5a). Crystals (up to 100 µm across) are short prismatic, with little or no preferred orientation. Garnet composition varies within the zone from *c.* Adr_{55}–Grs_{45} on the Z1 side to nearly pure grossular in the middle of the zone, and then remains unchanged to Z3 (Table 1; Supplementary Material, Fig. S2). Locally, short en échelon veinlets have opened in zone Z2 and are filled with white fibres of monomineralic wollastonite. Single-crystal diffraction data point to the simultaneous presence of the two main polytypes of wollastonite, the triclinic 1*A* (with its twin-related counterpart) prevailing over the monoclinic 2*M* (S. Merlino, personal communication, 2009). Zones Z1 and Z2 are both cross-cut by narrow serpentine-filled cracks, which therefore postdate the contact zone formation.
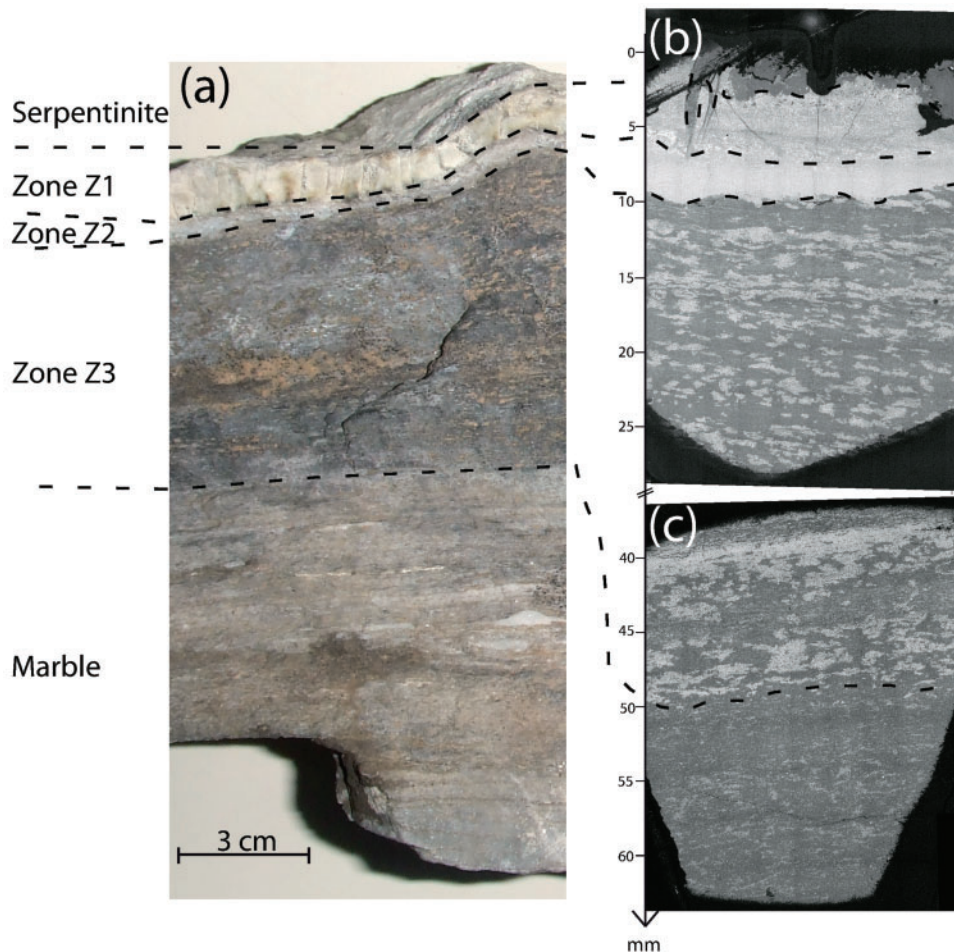
Fig. 4. A section through the reaction zone between serpentinite and marble. (a) Photograph of sample 09-04; the reaction zone is divided into layers (Z1–Z3) as described in Fig. 2 and the text. The darker colour of zone Z3, the lighter colour of zone Z2 and the jade-like, 'nephritic' aspect of zone Z1 should be noted. (b, c) BSE images of whole thin sections prepared from a slice cut through sample 09-04 [perpendicular to the plane of (a)], the top of (b) being in contact with serpentinite, and the bottom of (c) in contact with marble. [Note the difference in scale between (a) and (b, c), as well as the difference in colour and texture from one zone to another, reflecting changes in chemistry and mineral content as indicated in Figs 5 and 6.]

Zone Z3

The texture of zone Z3 is similar to that of the marble but the rock is made of $c.$ 70% quartz and 30% prismatic wollastonite oriented in the marble layering (Figs 4 and 5a, d). Small amounts of elongated grossular garnet (Table 1) and rare pectolite, $NaCa_2Si_3O_8(OH)$, are also observed. As mentioned above, zone Z3 is remarkable for its dark colour. Optical microscopy as well as SEM secondary-electron images and micro-Raman spectroscopy (Galvez et al., in preparation) show that graphitic matter is responsible for the darkness of this zone.

Modal and chemical changes across the reaction zone

The bulk-chemistry of the various zones was determined by averaging the results of EDS mapping (3 μm pixels) on a mesh of 3 mm length parallel to the profile and 3 cm width perpendicular to the profile; mineral modes were derived from elemental X-ray mapping coupled with image analysis (see 'Analytical methods'). Bulk composition data are given normalized to the mole percentage of the cations (i.e. the molar percentages of all the analyzed cations sum to 100%). The corresponding results are displayed in Fig. 6 and in the Supplementary Material (Table S1).

From the serpentinite contact towards the marble, Mg and Al molar concentrations are both reduced by a factor of $c.$ 2·5 (Fig. 6c). In contrast, Ca and Fe show a marked concentration increase. The decoupling between Mg and Fe at the serpentinite–Z1 interface can be explained by the presence of andradite in Z1, which hosts trivalent iron and no magnesium, magnesium being mostly concentrated in diopside in this zone (Fig. 6). Beyond Z1, the aluminium concentration is relatively constant ($c.$ 1·3 mol %); small
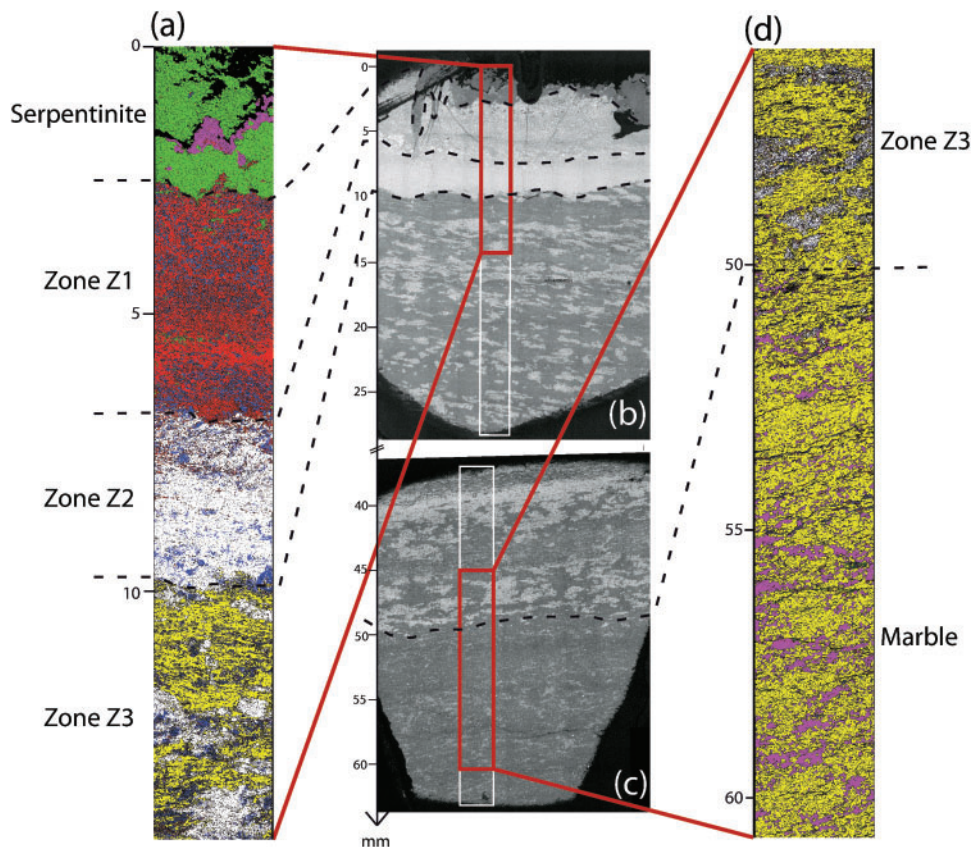
Fig. 5. (a to d) Anatomy of the reaction zone between serpentinite and marble. (b, c) BSE images of two thin sections from sample 09-04 (as indicated in Fig. 4b and c). (a, d) Selected parts [red rectangles in (b) and (c)] of profiles obtained from EDS mapping and BSE images show the variations in mineral content across the reaction zone. Green refers to serpentine, violet to calcite, red to clinopyroxene, blue to garnet, white to wollastonite, yellow to quartz, and dark green to mica.

Al variations are correlated with changes in the Ca/Si ratio, which may therefore represent initial heterogeneity in the former carbonate sediment. The Mg, Fe and Mn concentrations are below the EDS detection limit beyond Z2. The Si and Ca concentrations are roughly constant through zones Zl and Z2 (*c.* 45 and 35 mol %, respectively) whereas at the contact between zones Z2 and Z3 Si strongly increases whereas Ca, like most elements, strongly decreases. Beyond that contact, Ca and Si concentrations display inverse trends owing to the fact that Ca and Si are held by the two most abundant minerals, either wollastonite and quartz or calcite and quartz in the marble. For example, in zone Z3, the wollastonite 'mode' (surface area) is between 5 and 80% and is complementary to that of quartz (Fig. 6b).

Variations in the relative proportions of calcite and quartz in the marble are probably related to compositional heterogeneities of sedimentary origin. Similar Ca/Si variations in Z3 may have the same origin and therefore be a first hint that wollastonite replaced calcite in that zone. This assumption is supported by the chemical continuity,

at first order, between the dark zone Z3 and the marble. Upon closer examination, the transition between zone Z3 and marble is marked by a drop in potassium concentration. This drop coincides with the appearance of garnet, thereby defining a cryptic subzone in the marble, next to zone Z3, characterized by the presence of garnet and the near-absence of mica. The aragonite–grossular-bearing sample studied by Chopin *et al.* (2008) is a lateral equivalent of this subzone.

Identifying the main reactions

Formation of wollastonite in the reaction zone

One of the most striking observations in the contact zone is the abrupt disappearance of calcite coupled with the appearance of graphitic matter (GM) and wollastonite to form a marked dark reaction zone (Z3). The reaction front is *c.* 1·5 mm thick. Figure 7 shows the textural relationship between quartz, calcite, wollastonite and GM at the marble/Z3 contact. Lath-shaped crystals of wollastonite seem to replace calcite (Fig. 7b and c) and their crystallization is accompanied by GM formation (Fig. 7c).
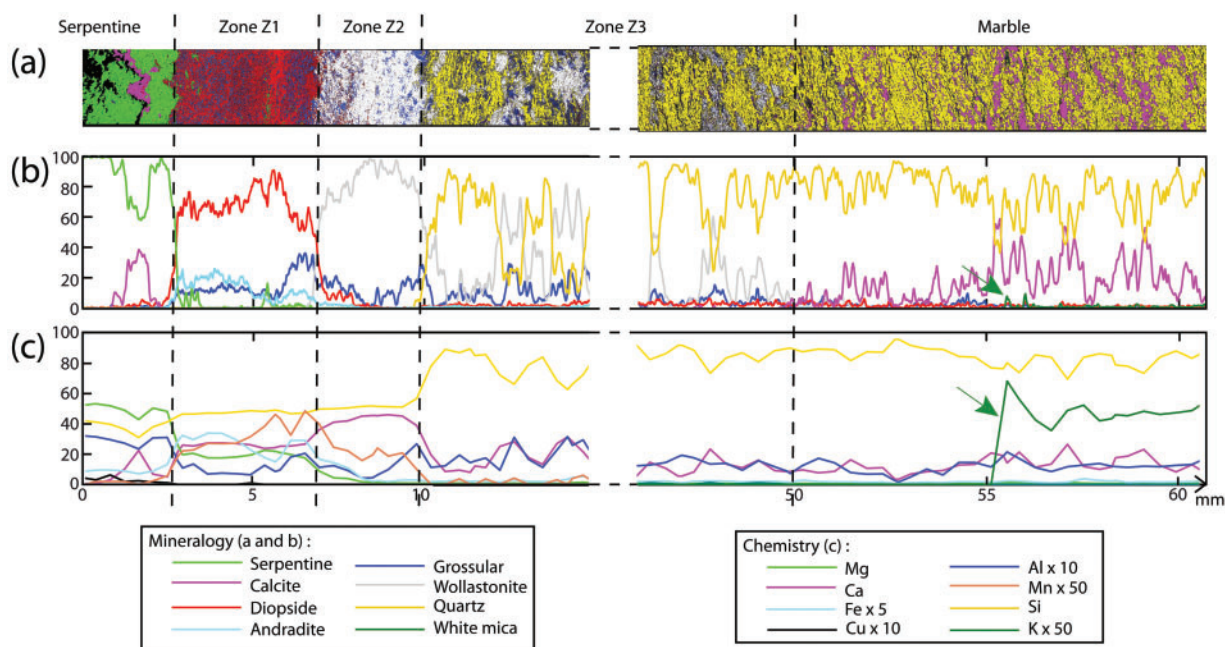
Fig. 6. Profiles through the reaction zone (sample 09-04). (a) Mineralogical mapping across selected boundary areas (reproduced from Fig. 5a and d for reference). (b) Mineral and garnet end-member modes across the reaction zone. The changes associated with each zone boundary and the presence of white mica only in the marble should be noted. Calcite in the serpentinite is a late cross-cutting vein. (c) Chemistry as determined by integration (on 3 μm stripes) of the EDS maps across the profile. Values are in molar proportions of the cations. The high concentrations in Mn, Fe and Mg in zone Zl, and the presence of K (in phengite - green arrows) only in the distal part of the marble (with respect to serpentinite) should be noted.

The size of the wollastonite grains increases towards Z2 concomitantly with GM content (Fig. 7b). Moreover, the texture of the wollastonite + quartz assemblage in zone Z3 is very similar to the texture of the calcite + quartz zone in the marble. We take all these observations, in particular the coincidence of carbon enrichment (the dark halo) with wollastonite appearance and calcite disappearance, as compelling evidence that zone Z3 arose from the progression of the following decarbonation reaction into the original marble, by which carbonate is reduced directly to produce elemental carbon:

$$SiO_2 + CaCO_3 = CaSiO_3 + C + O_2^f \qquad (1)$$

which may also be written, considering water dissociation,

$$SiO_2 + CaCO_3 + 2\,H_2^f = CaSiO_3 + C + 2\,H_2O^f. \quad (1b)$$

Given the stability of calcite + quartz everywhere else in the series and the metamorphic pile, the progress of this reduction reaction must imply the presence of an unusually reducing fluid.

The TOC (total 'organic' content) in marble sample 09-04 ranges from 0·22 to 0·34 wt % with the higher value close to Z3. In contrast, TOC in Z3 from the same sample ranges from 5·2 to 2·88 wt % with the lower value close to Z2. The amount of elemental carbon that could be produced by decomposition of calcite in Z3 following

reaction (1) is 3·0 wt %. This value is consistent with the 3·7 wt % average difference between the TOC content in each zone, thus supporting the idea that marble calcite can be the main carbon source for GM enrichment in zone Z3 (i.e. the dark halo). A detailed chemical and isotopic study coupled with micro-Raman characterization (Galvez et al., in preparation) confirms this point and thoroughly addresses the effectiveness and the mechanisms of this uncommon formation of elemental carbon.

A garnet-forming reaction in the marble

The chemical profile from marble to serpentinite provides an answer to the question left pending by Chopin et al. (2008), namely that of the garnet-forming reaction in the marble, and its localization to the immediate vicinity of the serpentinite (higher in the series, the marble is free of garnet). Potassium, which is absent from the reaction zone (Fig. 6c), is hosted by white mica in the original marble. At the zone Z3–marble contact, white mica is surrounded by garnet (Fig. 7d) and is no longer observed in the Zl–Z3 reaction zone, but it may have been initially present in the parts that represent former marble; that is, Z3 (as shown above) and most probably Z2 (see below). Actually, in zones Z2 and Z3 where white mica is now absent, garnet displays lamellar morphologies mimicking a mica habit (Fig. 8). The combination of textural and chemical information with respect to potassium therefore
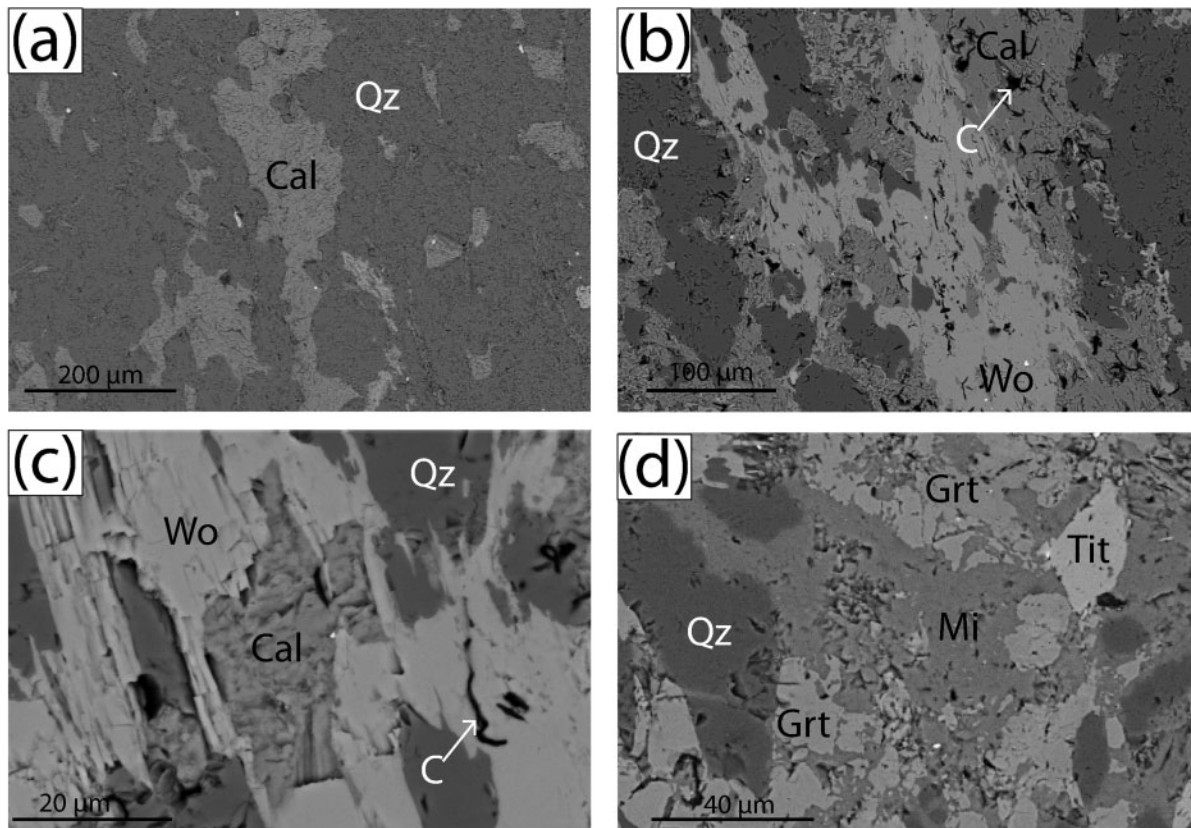
Fig. 7. BSE images illustrating the occurrence of wollastonite and garnet within the marble exclusively at the serpentinite–marble interface. (a–c) Wollastonite (+ graphitic matter) appearance (sample 09-04): comparison of texture in 'unreacted' siliceous marble (a) and in the boundary zone (b) where wollastonite appears within marble (i.e. at the marble–Z3 interface). The abundance of a black phase interpreted as carbon in (b) compared with (a) should be noted. (c) Close-up showing calcite 'armoured' by wollastonite in a wollastonite + quartz groundmass in the narrow (*c.* 1·5 mm) transition zone where calcite, quartz, wollastonite and carbon coexist (sample 09-04). (d) Garnet in siliceous marble (sample 09-05) close to the marble–Z3 boundary. The concomitant presence of white mica (Mi), quartz and garnet is proposed as evidence for reaction (2). (See also Fig. 8.)

suggests that the disappearance of white mica is coupled to potassium leaching and garnet growth, and to the unusual conditions prevailing near the contact with the serpentinite. On this basis and taking Ca-carbonate reduction into account, a tentative dissolution reaction can be proposed as follows:

$$2 \, KAl_3 \, Si_3 \, O_{10}(OH)_2 + 3 \, SiO_2 + 9 \, CaCO_3 + 2 \, H^+ = \atop 3 \, Ca_3Al_2 \, (SiO_4)_3 + 2 \, K^+ + 9 \, C + 9 \, O_2 + 3 \, H_2O \quad (2)$$
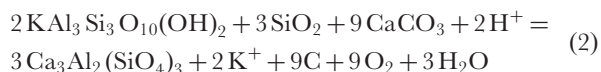
which is pH and $f\mathrm{O}_2$ dependent and also produces elemental carbon.

Formation of zones Z2 and Z1; locating the former interface
The Si content decreases by a factor of two from Z3 (and marble) to Z2 (and Z1) as indicated by the disappearance of quartz. In Z2, the Ca/Si molar ratio reaches that of wollastonite, the main Z2 mineral that contains both Ca and Si cations. Consequently, Z2 is, to the first order, equivalent to zone Z3 that has entirely lost its quartz component.

Therefore in the framework of a reaction process between two contrasted lithologies (serpentinite and siliceous marble), Z2 would be of marble affinity. In comparison, Z1 appears as totally different with higher Si/Ca, Fe/Ca and Mg/Ca ratios, more consistent with a serpentinite affinity. The original interface between serpentinite and marble has been overprinted; it must, however, have been located between the serpentine and the wollastonite fronts (i.e. within the present zone Z1).

Formation of uvarovite–andradite garnet in the serpentinite
In serpentinite, subordinate garnet is uvarovite–andradite in composition; this occurs in aggregates along with Fe–Cr oxides and Cr-rich chlorite in the presence of clinopyroxene. This textural relationship suggests that the aggregates replace a former Fe–Cr–Al spinel, which reacted with clinopyroxene to form Cr-rich garnet ± chlorite (Fig. 4). Interestingly, this type of reaction is accompanied by the oxidation of the Fe^{2+} present in Fe–Cr oxides into Fe^{3+} in the andradite component, which represents
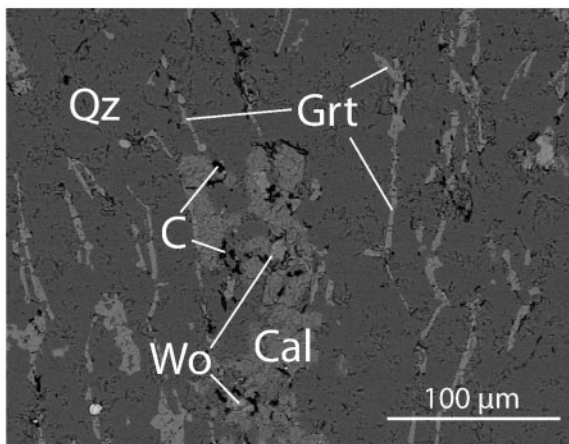
Fig. 8. BSE image showing the texture of the boundary zone between marble and Z3. The presence of wollastonite and carbon and the lamellar growth of garnet, mimicking the habit of mica in the marble, should be noted. Garnet occurs with the same lamellar shape within zone Z3 but is difficult to observe in BSE images because of its similarity to wollastonite in backscattering power.

45 mol % of the garnet. Assuming that this garnet formed during subduction metamorphism, its formation contributed to fuelling the redox potential of the serpentinite during metamorphism.

QUANTIFICATION OF THE REDOX CONDITIONS DURING SERPENTINITE–MARBLE INTERACTION

In the previous section, a series of zones with contrasting mineralogy and chemistry were described, which occur at the contact between a serpentinite and a marble unit and formed under blueschist-facies conditions. The presence of wollastonite in such a low-temperature terrane, in association with GM, is interpreted as resulting from calcite reduction in the presence of quartz and a reducing fluid. In the following sections, thermochemical modelling is used to constrain the oxygen fugacity that prevailed during serpentinite–marble interaction and that, apparently, reached a low enough value to trigger carbonate reduction.

Databases and modelling methods

Equilibrium constants of reaction were calculated for various P and T from reaction Gibbs free energy calculated with the database of Holland & Powell (1998; 2002 update). Equilibrium constants involving aqueous species and gas fugacities [e.g. reaction (1)] were determined with SUPCRT92 (Johnson *et al.*, 1992) with the limitation that the Gibbs free energy of aqueous species cannot be calculated for pressures above 0·5 GPa with this software. Consequently, this computational limitation does not allow us to model equilibrium at the conditions

experienced here; however, the effect of pressure on equilibrium constants was found to be negligible compared with the impact of temperature and uncertainty on them.

Stable mineral and fluid–mineral associations for a given bulk composition (in a given P–T range) were calculated using PerpleX (Connolly, 1990, 2005; Connolly & Petrini, 2002). The modelled system was assumed to be graphite-saturated. The mixed equations of state for O_2, H_2O and CO_2 from Connolly & Cesare (1993) were used. The amount of H and O atoms in the modelled system was not fixed but taken as a variable through the X_O parameter; that is, the number of oxygen atoms in the fluid divided by the number of oxygen plus hydrogen atoms in the fluid, at graphite saturation (Connolly, 1995). Therefore X_O is a purely compositional variable in the C–O–H system, with no bearing on speciation. Even though the Gibbs free energy minimization performed by PerpleX fails to retrieve oxygen fugacity (oxygen contents being far too low), the oxygen fugacity (and fluid composition) in a carbon-saturated system can be recalculated for a given X_O value using appropriate equilibrium constants (Connolly, 1995). The solid-solution model for clinopyroxene is taken from Holland & Powell (1996). For thermochemical computation, the graphitic material is considered here to be graphite (see Galvez *et al.*, in preparation). All oxygen fugacities are given relative to the fayalite–magnetite–quartz buffer (FMQ) as ΔFMQ.

Modelling results

Across the reaction zone

The association wollastonite + quartz + GM, in the absence of calcite, sets an upper value to oxygen fugacity, which can be determined from the equilibrium constant of reaction (1) ($K_{E,1}$). As a result, for relevant conditions of pressure and temperature (e.g. 400–450°C at 1·5 GPa), maximum $f O_2$ conditions of $\sim\Delta$FMQ–1 are required to achieve calcite reduction (Fig. 9a).

The stability in $f O_2$–T–P space of the mineral assemblage andradite + diopside found in zone Z1 has also been investigated assuming equilibrium with a reducing fluid at graphite saturation (Connolly & Cesare, 1993; Connolly, 1995) although GM is no longer observed in Z1 (see Discussion). Both Al and Mn (respectively 0·8 and 0·5 mol %) were omitted from the bulk composition of zone Z1 determined by EDS, to limit the number of phases in the pseudosection (e.g. no grossular or chlorite); the bulk composition used for PerpleX modelling was therefore SiO_2 50·69, FeO 7·90, MgO 13·57, CaO 27·84 wt %. Figure 10a shows the result of a simulation performed at 1·5 GPa between 400 and 550°C (the geologically plausible range), as a function of fluid composition with X_O ranging from zero to 0·33. The andradite–diopside paragenesis (zone Z1) is found to be stable for X_O ranging from 0·001 to 0·32; that is, for redox conditions
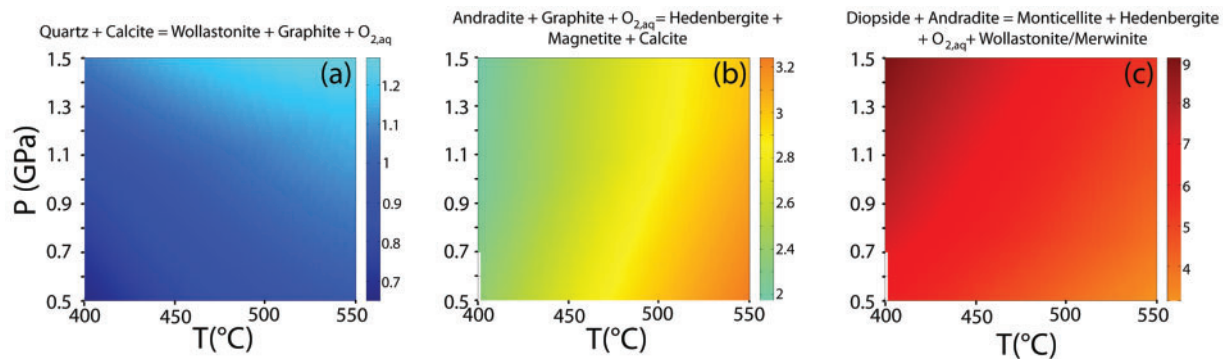
Fig. 9. Calculations of oxygen fugacity [scale in the colour codes is in $-\Delta FMQ \log(fO_2)$] for relevant buffer reactions in P–T space. (a) Reaction (1) pertaining to the boundary layer between marble and zone Z3. This provides the fO_2 value at a given P and T. (b) Reaction (3) relevant to zone Z1 (andradite + diopsidic pyroxene), providing an upper bound on fO_2. (c) Reaction (4) [or (5), depending on P], relevant to zone Z1, which provides a lower bound on fO_2. The solid-solution model by Holland & Powell (1996) was used for clinopyroxene assuming 3 mol % hedenbergite in diopside as estimated from electron microprobe analyses (Table 1).

corresponding to *c*. ΔFMQ–3 (Fig. 10b). For $X_O > 0.32$ (in the presence of GM), the alternative assemblage clinopyroxene + andradite + magnetite + Ca-carbonate is more stable according to the limiting reaction

$$12\,Ca_3Fe_2Si_3O_{12} + 18\,C + 13\,O_2, aq =$$
$$18\,CaFeSi_2O_6 + 2\,Fe_3O_4 + 18\,CaCO_3 \tag{3}$$
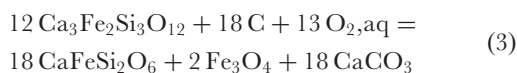
whereas, for $X_O < 0.001$ and depending on pressure, the association clinopyroxene + andradite + monticellite + wollastonite/merwinite is more stable as inferred from the limiting reaction

$$2\,CaMgSi_2O_6 + Ca_3Fe_2Si_3O_{12} =$$
$$CaSiO_3 + 2\,CaMgSiO_4 + 2\,CaFeSi_2O_6 + \frac{1}{2}\,O_2, aq \tag{4}$$

below 0.7 GPa, or

$$3\,CaMgSi_2O_6 + 2\,Ca_3Fe_2Si_3O_{12} =$$
$$Ca_3Mg(SiO_4)_2 + 2\,CaMgSiO_4 + 4\,CaFeSi_2O_6 + O_2, aq \tag{5}$$
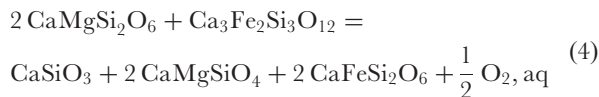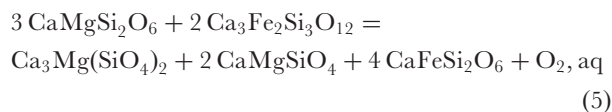
above 0.7 GPa.

Equilibrium constants for these reactions were determined over a wide range of pressures and temperatures, to scan the whole spectrum of compatible fO_2 conditions (Fig. 9). A maximum oxygen fugacity of *c*. ΔFMQ–2.6 ($\pm$ 0.6) is implied by the stability of andradite vs hedenbergite + magnetite + calcite (Fig. 9b). On the other side, reactions (4) and (5) provide a lower bound on fO_2, the stability of andradite + diopside vs hedenbergite + monticellite + wollastonite/merwinite implying redox conditions above ΔFMQ–7 ($\pm$ 2, depending on P and T) (Fig. 9c).

If saturation of the aqueous fluid phase with respect to GM is postulated, then the fluid-mediated interaction between serpentinite and marble under reducing conditions, already inferred from calcite reduction (Z3), is confirmed

by the mineral assemblage of Z1. It should be noted that under the redox conditions calculated with PerpleX at graphite saturation for zone Z3, the equilibrium fluid is indeed reducing and is characterized by large proportions of CH_4 and H_2 (Fig. 10c).

Important issues with respect to determination of the redox conditions that prevailed during the growth of the reaction zones are the evolution of the carbon distribution (either as carbonate or as GM) and the saturation of the fluid with respect to GM. Carbon is present in the form of carbonate (along with some GM) in the pristine marble whereas it occurs solely as GM in Z3. The location of the original serpentine–marble interface within Z1 suggests that carbon was initially present also in Z2 and in part of zone Z1, where it is no longer observed. By what process has carbon been removed? Under the reducing conditions calculated above for the contact zone, a likely means for carbon removal is the formation of CH_4 molecules, which are definitely more mobile than solid GM. Consequently, the fluid that reduced zones Z1 and Z2 and stripped away any GM must have had a higher H_2 content than zone Z3 fluid, pointing again to a redox gradient (or reduction front) across the contact zone, with the most reducing conditions prevailing on the serpentinite side.

Redox potential of a fully serpentinized peridotite

The redox conditions modelled here and the areal distribution of the wollastonite–GM halo point to the reducing effect of the serpentinite body during metamorphism. In the serpentinite the coexistence of Co-bearing pentlandite and magnetite is the only constraining assemblage with respect to oxygen fugacity. Klein & Bach (2009) have shown that, considering the whole range of H_2S fugacities, the field of coexistence of these phases at 400°C and 500 bars is only limited towards high oxygen fugacity by the hematite–magnetite equilibrium. Consequently, in the absence of Fe–Ni alloys, the ambient oxygen fugacity of the
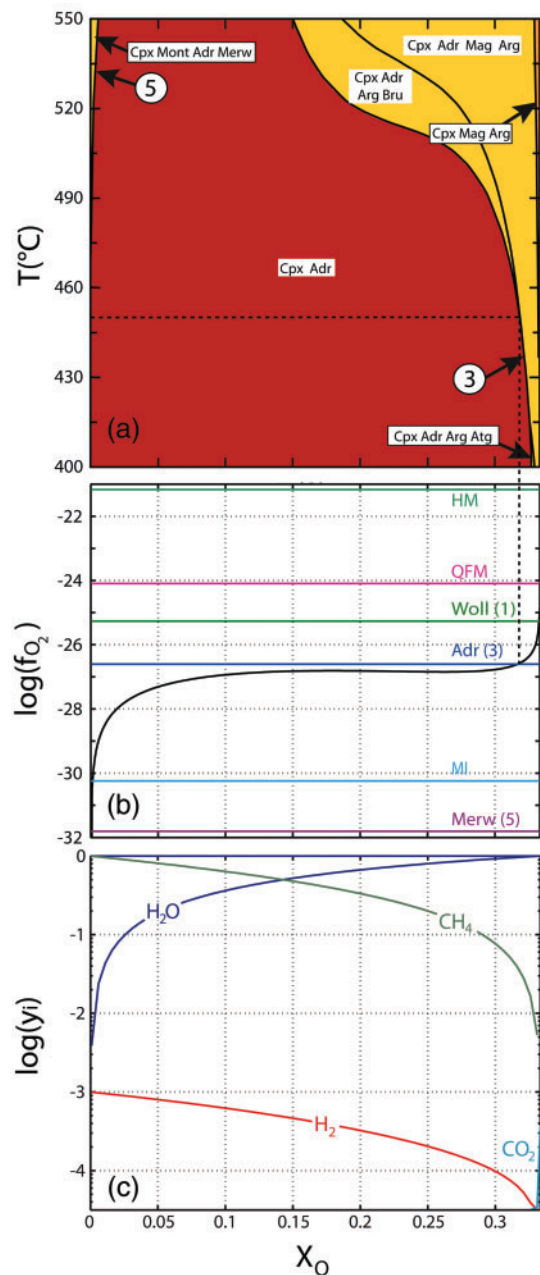
Fig. 10. Thermochemical isobaric modelling for the simplified bulk composition of zone Z1 (andradite + diopsidic pyroxene), as a function of X_O at carbon saturation, where X_O is the molar ratio $O/(O+H)$ in the fluid [$P = 1.5$ GPa; $X_{Fe^{2+}}$(cpx) = 0.03]. (a) Stable assemblages as a function of T and X_O. The assemblage observed in Z1 (andradite + clinopyroxene) is shown in red, bounded by three other parageneses. Considering the limits of this field at a given T provides an upper [reaction (3)] and a lower [reaction (5)] bound on oxygen fugacity at the base of zone Z1 (i.e. on the serpentinite side, where garnet is near-end-member andradite). (b) X_O vs log(fO_2) diagram calculated at 450°C and 1.5 GPa showing (black line) the oxygen fugacity of the equilibrium COH fluid at carbon saturation, and the oxygen fugacities imposed by a variety of buffer reactions under the same P–T conditions (labelled lines): HM, hematite–magnetite; QFM, quartz–fayalite–magnetite; Woll, reaction (1); Adr, reaction (3); MI, magnetite–iron; Merw, reaction (5). (c) Chemical concentration of the main species in the fluid phase at carbon saturation as a function of X_O at 450°C and 1.5 GPa, calculated with PerpleX. For $X_O = 0.2$, log(CO_2) = −4.76 and log(CO) = −7.62.

serpentinite is difficult to constrain. It is now well established that peridotites have a strong reducing potential (Berndt *et al.*, 1996; Charlou, 2002; Seyfried *et al.*, 2007; Evans, 2010; Marcaillou *et al.*, 2011). However, the reducing effect of a fully serpentinized body that could further interact with aqueous fluids (i.e. post-serpentinization interaction) has not been investigated so far. In addition to uvarovite–andradite garnet formation, for which thermodynamic data are lacking, a reaction that can account for the reducing potential of the serpentinite is the following serpentine–magnetite equilibrium:

$$3Fe_3Si_2O_5(OH)_4 + 2O_{2,aq} = 3Fe_2\square Si_2O_5(OH)_4 + Fe_3O_4. \tag{6}$$
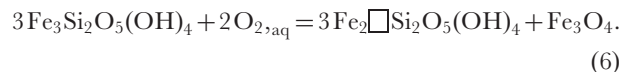
The equilibrium constant of (6) at 450°C and 0.5 GPa (K_{E6}) was calculated with the thermodynamic database of Klein et al. (2009) and the SUPCRT92 software (Johnson et al., 1992) to relate the Fe^{3+}/Fe^{2+} ratio in serpentine and oxygen fugacity ($K_{E6} = 10^{57.5}$). Through this reaction, the oxidation of serpentine from ΔFMQ–4 (i.e. oxygen fugacity of a natural serpentinite; Frost, 1985; Frost & Beard, 2007; Evans, 2008) to ΔFMQ–1 [i.e. maximum fO_2 at which carbonate is no longer reduced according to reaction (1)] results in the formation of magnetite with an O_2 uptake of 0.008 mole of O_2 per mole of serpentine. Assuming that this O_2 entirely comes from the reduction of $CaCO_3$ in the neighbouring marble, then 1 g of $CaCO_3$ can be reduced by 350 g of a serpentine initially equilibrated at ΔFMQ–4. This simple mass-balance calculation supports the field evidence that a fully serpentinized peridotite entrained in a subduction zone has still the potential to reduce carbonates in the nearby sedimentary formations.

DISCUSSION
Conditions and processes of formation of the reaction zone

The reaction zone studied here between serpentinite and marble is located in metamorphic units that experienced pressures and temperatures of the order of 1–2 GPa at 450–500°C (Lahondère, 1996; Chopin *et al.*, 2008). The presence of high-Si phengite in marble imposes minimum pressures of about 1.5 GPa (Massonne & Schreyer, 1987; Coggon & Holland, 2002); continuing RSCM thermometry studies in the area indicate temperatures closer to 425°C (Vitale-Brovarone *et al.*, in preparation; Galvez *et al.*, in preparation). Garnet formed during the interation between serpentinite and marble has trapped aragonite inclusions (Chopin *et al.*, 2008); therefore, the reaction zone must have formed at metamorphic, high-pressure and low-temperature conditions. The thickness of the reaction zone implies transport of species over several centimetres (or even tens of centimetres). This transport must have

been promoted by the presence of a fluid that, in the context of high-P, low-T metamorphism of serpentinite, is likely to have been mostly aqueous. In addition, the reduction of Ca-carbonate (either calcite or aragonite) in the presence of quartz to form wollastonite $+$ GM indicates that this aqueous fluid was reducing and imposed redox conditions below ΔFMQ–1.

The assumption of a reaction process dominated by diffuse transport rather than fluid advection underlies this study; it is apparently challenged by the potassium profile, which could suggest potassium leaching in the marble by aqueous fluid flow. Potassium dissolution can be accounted for by reaction (2), the equilibrium constant (K_{E2}) of which depends on the potassium, water and oxygen activities as well as the pH of the aqueous fluid, in addition to P and T, as follows:

$$K_{E2}(P,T) = (a_{K^+}^2 * a_{O_2}^9 * a_{H_2O}^3)/(a_{H^+}^2).$$

Potassium concentration in the marble can be used to constrain the minimum fluid/rock ratio needed to dissolve all the potassium out of the rock. This fluid/rock ratio is highly dependent on oxygen fugacity as its exponent is nine in this equation. Using the low oxygen fugacity determined previously (ΔFMQ–1 to -3) and the K_{E2} (0·5 GPa, 450°C) value calculated with SUPCRT92 (Johnson *et al.*, 1992), it turns out that a very small water/rock ratio (of the order of 10^{-5} litres of H_2O per kg rock at 0·5 GPa, 450°C, ΔFMQ–2 and pH 6) is sufficient to entirely dissolve the potassium of white mica (0·85 mol % of the rock) under these conditions. However, this calculation is also strongly temperature dependent (10^5 litres of H_2O per kg rock are required at 400°C) and extrapolation to higher pressures is fraught with uncertainty. Consequently, the calculation only shows that repeated renewal of the pore fluid or constant fluid flow is not necessarily required to account for most of the reaction features of the contact zone, as decreasing the oxygen fugacity strongly increases potassium solubility. This is in line with the unusual lamellar texture of garnet (replacing mica) in zone Z3, suggesting very limited mass transfer. Therefore, the view of Fickian diffusion in an almost stagnant fluid medium may be retained here for simplicity. There is indeed no clear evidence that deformation-triggered advection took place in these rocks under the near-climax metamorphic conditions during which the reaction zone developed. On this basis, we can tentatively interpret the formation of the reaction zone as the result of chemical potential gradients between serpentinite and marble in the presence of an intergranular fluid, which enhances species diffusion (Rubie, 1986; Baxter, 2003). The division of the contact zone into three reaction zones (Z1, Z2 and Z3) results in the decoupling of the species transport kinetics through contrasted apparent diffusion coefficients for H_2, O_2, CH_4, SiO_2, CaO, MgO, etc. The steep concentration gradient observed at the interface between each of the reaction zones reveals an overall diffusion-controlled process where precipitation, crystallization and reaction kinetics are not limiting factors. Among the obvious chemical potential gradients that have driven the formation of the reaction zones, the one imposed by contrasted oxygen fugacity between serpentinite and marble is remarkable, as it led to the reduction of calcite and to the low-temperature formation of wollastonite and elemental carbon, three rare features in metamorphic environments. Another major boundary condition is the gradient in silica activity between silica-undersaturated serpentinite (with perovskite) and siliceous marble; silica diffusion between them, across the quartz-free wollastonite zone (Z2), may be a limiting factor for the growth of the rodingite rim (Z1).

It is also worth noting that redox gradients, here, are not independent of the chemical potential gradient of other components. For example, part of the ferrous iron from the serpentinite is transferred to Z1 and part of Z2 as ferric iron in andradite. Consequently, andradite formation contributes to maintaining a low fO_2 on the serpentinite side. Mass-balance calculations are now required to determine whether the oxygen fugacity gradient across the contact zone could be self-sustained, at least in a transient way, by the coupled formation of andradite in Z1 after having been only sparked off by the reducing conditions of the serpentinite.

Another feature of the reaction zone is the high Ca content in Z1 and Z2, which is classical for rodingite. In other rodingites, this enrichment has been linked to serpentinization and chloritization of the primary clinopyroxene of the peridotite and to fluid transport in fracture zones (Austrheim & Prestvik, 2008). In the Malaspina serpentinite, even though clinopyroxene is concentrated in foliation planes, there is no evidence of Ca release associated with rodingitization. In this case, however, the country-rock marble at the contact is the most obvious Ca reservoir and source.

Low-temperature wollastonite: a marker for reducing fluids? Review of other occurrences

This study shows that wollastonite and elemental carbon can form through calcite or aragonite decarbonation at low temperature if sufficiently reducing (CO_2-free) conditions are achieved. Reports of wollastonite in low-grade terranes are, with one exception (Markl, 1999), all linked to serpentinites. In the Western Alps, Amstutz (1962) and Di Colbertado *et al.* (1967) mentioned wollastonite in marbles at the contact with the Cogne serpentinite body. However, there is no mention of abundant graphite and these early reports are now questioned (Piccoli *et al.*, 2007; R. Compagnoni, personal communication, 2010). As in the

Western Alps (Dal Piaz, 1969), rodingites also occur in the Franciscan Complex of California and Oregon (e.g. Coleman, 1967). In serpentinites at Cape San Martin and Leech Lake Mountain, CA, both in greywacke country-rock, fibrous masses and veins of wollastonite were found, respectively, by Gresens (1966) and in a sample collected by S. O. Agrell and included in Wenk's (1969) crystallographic study. This sample, which we re-examined on loan from the Harker Collection, Cambridge University, UK, shows anastomosing millimetre-size veins of wollastonite with sparse grains (>100 μm) of andraditic grossular, cross-cutting a matrix of transformed greywacke made of diopside and grossular (c. 10 μm grain size for both). This sample can be safely ascribed to the reaction zone described along the serpentinite–country-rock contact (see the photograph of Chesterman, 1960), by analogy with the profiles studied by Coleman (1967) on the margin of other Franciscan ultramafic bodies. Similar occurrences of wollastonite in rodingite are known from the Kamiukotan belt, Hokkaido (Katoh & Niida, 1983), and the JM Asbestos mine, Québec, where fluid inclusions contain CH_4 (probably deriving from a serpentinization fluid; Normand & Williams-Jones, 2007). Xonotlite, $Ca_6Si_6O_{17}(OH)_2$, a low-temperature hydrated equivalent of wollastonite, was also found in rodingites from New Zealand (O'Brien & Rodgers, 1973) and in the Ronda massif, Spain, where carbonaceous material is also observed (Esteban et al., 2003).

Therefore, wollastonite does occur at low temperatures, but almost exclusively in reaction zones in and around serpentinites. In the Franciscan, Kamiukotan, New Zealand and Québec examples, the absence of carbonates in the country-rock does not allow one to use the maximum fO_2 indicator offered by their stability versus elemental carbon + wollastonite. On the other hand, some carbonate–serpentinite contacts in the Alps or Corsica do not show a reaction zone. This may reflect the difference between relatively early contacts with continuously traceable reaction zones (e.g. Malaspina or Leech Lake Mountain) and late tectonic contacts where no such reaction happened, either for kinetic reasons or because the serpentinite had lost its reducing potential. Interestingly, late calcite veinlets cross-cutting the Malaspina reaction zone (Fig. 6) did not react with quartz, suggesting less reducing conditions during the latest stages of the tectono-metamorphic evolution. In other serpentinite bodies, the development of carbonate-rich alteration zones (compare listvenite) points to a much more open-system behaviour and to pervasive flow of more oxidizing, CO_2-rich, externally derived fluids (e.g. Tsikouras et al., 2006; Beinlich et al., 2010). In contrast, the reduction in and around the serpentinite in this study is associated with diffusion of a fluid with a low water/rock ratio.

Serpentinite as a reducing environment: implication for redox conditions in subduction zones

It is well established that serpentinization of oceanic peridotites near slow-spreading centres produces highly reducing fluids containing dissolved H_2 resulting from the reduction of H_2O (Berndt et al., 1996; Charlou, 2002; Seyfried et al., 2007; Klein & Bach, 2009; Klein et al., 2009; Marcaillou et al., 2011). In contrast, there is no consensus on the redox conditions in subduction zones. Arc lavas studies (Arculus, 1994; Stolper & Newman, 1994), geochemistry and fluid inclusion studies in mantle xenoliths (Parkinson & Arculus, 1999; Andersen & Neumann, 2001), iron distribution in garnet from orogenic peridotites (Malaspina et al., 2009), and study of the Fe^{3+}/Fe ratio in basaltic glasses and melt inclusions (Kelley & Cottrell, 2009) tend to show that these zones are oxidized, whereas Zn/Fe ratios (Lee et al., 2010) and other fluid inclusion data (Song et al., 2009) suggest that they are reduced. Our study shows that subducting serpentinites can impose reducing conditions (oxygen fugacities below ΔFMQ–1). Moreover, the thermochemical modelling presented here indicates that in situ serpentinization of anhydrous peridotite during subduction-zone metamorphism is not required to generate reducing conditions. Both during oceanic hydrothermal alteration and later in the subduction zone, reducing conditions far below ΔFMQ can be reached during metamorphism in and around pre-serpentinized ultramafic bodies, as revealed by the occurrences of low-T wollastonite and graphitic material, which imply the presence of H_2- and possibly CH_4-bearing aqueous fluids.

ACKNOWLEDGEMENTS

SUPPLEMENTARY DATA

Supplementary data for this paper are available at *Journal of Petrology* online.

REFERENCES

Amstutz, A. (1962). Notice pour une carte géologique de la vallée de Cogne et de quelques autres espaces au sud d'Aoste. *Archives des Sciences (Société de Physique et d'Histoire Naturelle de Genève)* **15**, 1–104.

Andersen, T. & Neumann, E. R. (2001). Fluid inclusions in mantle xenoliths. *Lithos* **55**, 301–320.

Arculus, R. (1994). Aspects of magma genesis in arcs. *Lithos* **33**, 189–208.

Austrheim, H. & Prestvik, T. (2008). Rodingitization and hydration of the oceanic lithosphere as developed in the Leka ophiolite, north–central Norway. *Lithos* **104**, 177–198.

Auzende, A. L., Daniel, I., Reynard, B., Lemaire, C. & Guyot, F. (2004). High-pressure behaviour of serpentine minerals: a Raman spectroscopic study. *Physics and Chemistry of Minerals* **31**, 269–277.

Baxter, E. F. (2003). Natural constraints on metamorphic reaction rates. In: Vance, D., Müller, W. & Villa, I. (eds) *Geochronology: Linking the Isotopic Record with Petrology and Textures. Geological Society, London, Special Publications* **220**, 183–202.

Beinlich, A., Austrheim, H., Glodny, J., Erambert, M. & Andersen, T. B. (2010). CO_2 sequestration and extreme Mg depletion in serpentinized peridotite clasts from the Devonian Solund basin, SW Norway. *Geochimica et Cosmochimica Acta* **74**, 6935–6964.

Berndt, M. E., Allen, D. E. & Seyfried, W. E. (1996). Reduction of CO_2 during serpentinization of olivine at $300°C$ and 500 bar. *Geology* **24**, 351–354.

Caron, J. M. & Péquignot, G. (1986). The transition between blue-schists and lawsonite-bearing eclogites based on observations from Corsican metabasalts. *Lithos* **19**, 205–218.

Charlou, J. (2002). Geochemistry of high H_2 and CH_4 vent fluids issuing from ultramafic rocks at the Rainbow hydrothermal field (36°14′N, MAR). *Chemical Geology* **191**, 345–359.

Chesterman, C. W. (1960). Intrusive ultrabasic rocks and their metamorphic relationships at Leech Lake Mountain, Mendocino County, California. *21st International Geological Congress, Copenhagen, Proceedings* **13**, 208–215.

Chopin, C., Beyssac, O., Bernard, S. & Malavieille, J. (2008). Aragonite–grossular intergrowths in eclogite-facies marble, Alpine Corsica. *European Journal of Mineralogy* **20**, 857–865.

Coggon, R. & Holland, T. J. B. (2002). Mixing properties of phengitic micas and revised garnet–phengite thermobarometers. *Journal of Metamorphic Geology* **20**, 683–696.

Coleman, R. G. (1967). *Low-temperature reaction zones and Alpine ultramafic rocks of California, Oregon and Washington. US Geological Survey Bulletin* **1247**, , 49 p.

Compagnoni, R., Ferraris, G. & Fiora, L. (1983). Balangeroite, a new fibrous silicate related to gageite from Balangero, Italy. *American Mineralogist* **68**, 214–219.

Connolly, J. A. D. (1990). Multivariable phase diagrams; an algorithm based on generalized thermodynamics. *American Journal of Science* **290**, 666–718.

Connolly, J. A. D. (1995). Phase diagram methods for graphitic rocks and application to the system $C–O–H–FeO–TiO_2–SiO_2$. *Contributions to Mineralogy and Petrology* **119**, 94–116.

Connolly, J. A. D. (2005). Computation of phase equilibria by linear programming: A tool for geodynamic modeling and its application to subduction zone decarbonation. *Earth and Planetary Science Letters* **236**, 524–541.

Connolly, J. A. D. & Cesare, B. (1993). C–O–H–S fluid composition and oxygen fugacity in graphitic metapelites. *Journal of Metamorphic Geology* **11**, 379–388.

Connolly, J. A. D. & Petrini, K. (2002). An automated strategy for calculation of phase diagram sections and retrieval of rock properties as a function of physical conditions. *Journal of Metamorphic Geology* **20**, 697–708.

Dal Piaz, G. V. (1969). Filoni rodingitici e zone di reazione a bassa temperatura al contatto tettonico tra serpentine e rocce incassanti nelle Alpi occidentali italiane. *Rendiconti della Società Italiana di Mineralogia e Petrologia* **25**, 263–316.

Deschamps, F., Guillot, S., Godard, M. & Chauvel, C. (2010). *In situ* characterization of serpentinites from forearc mantle wedges: Timing of serpentinization and behavior of fluid-mobile elements in subduction zones. *Chemical Geology* **269**, 262–277.

Di Colbertaldo, D., Di Furia, E. & Rossi, F. (1967). Il giacimento a magnetite di Cogne in Val d'Aosta. *Rendiconti dell'Istituto Lombardo–Accademia di Scienze e Lettere* **101**, 361–394.

Esteban, J. J., Cuevas, J., Tubía, J. & Yusta, I. (2003). Xonotlite in rodingite assemblages from the Ronda peridotites, Betic Cordilleras, Southern Spain. *Canadian Mineralogist* **41**, 161–170.

Evans, B. W. (2008). Control of the products of serpentinization by the $Fe^{2+}Mg_{-1}$ exchange potential of olivine and orthopyroxene. *Journal of Petrology* **49**, 1873–1887.

Evans, B. W. (2010). Lizardite versus antigorite serpentinite: Magnetite, hydrogen, and life (?). *Geology* **38**, 879–882.

Evans, B. W. & Kuehner, S. M. (2011). A nickel–iron analogue of balangeroite and gageite (Sasaguri, Kyushu, Japan). *European Journal of Mineralogy* **23**, 717–720.

Faure, F. & Malavieille, J. (1981). Etude structurale d'un cisaillement ductile: le charriage ophiolotique corse dans la region de Bastia. *Bulletin de la Société Géologique de France* **23**, 335–343.

Ferry, J. M., Wing, B. A. & Rumble, D., III (2001). Formation of wollastonite by chemically reactive fluid flow during contact metamorphism, Mt. Morrison pendant, Sierra Nevada, California, USA. *Journal of Petrology* **42**, 1705–1728.

Frost, B. R. (1985). On the stability of sulfides, oxides, and native metals in serpentinite. *Journal of Petrology* **26**, 31–63.

Frost, B. R. & Beard, J. S. (2007). On silica activity and serpentinization. *Journal of Petrology* **48**, 1351–1368.

Gresens, R. L. (1966). Wollastonite in rodingites from Cape San Martin, Monterey County, California. *Geological Society of America, Special Papers* **87**, (abstracts for 1965), 66–67.

Harlow, G. E., Sorensen, S. S. & Sisson, V. B. (2007). Jade. In: Groat, L. A. (ed.) *The Geology of Gem Deposits. Mineralogical Association of Canada, Short Course Series* **37**, 207–254.

Holland, T. J. B. & Powell, R. (1996). Thermodynamics of order–disorder in minerals: II. Symmetric formalism applied to solid solutions. *American Mineralogist* **81**, 1425–1437.

Holland, T. J. B. & Powell, R. (1998). An internally consistent thermodynamic data set for phases of petrological interest. *Journal of Metamorphic Geology* **16**, 309–343.

Iyer, K., Rüpke, L. H. & Morgan, J. P. (2010). Feedbacks between mantle hydration and hydrothermal convection at ocean spreading centers. *Earth and Planetary Science Letters* **296**, 34–44.

Katoh, T. & Niida, K. (1983). Rodingites from the Kamuikotan Tectonic Belt, Hokkaido. *Journal of the Faculty of Sciences, Hokkaido University, Series IV* **20**, 151–169.

Kelley, D. S., Karson, J. A., Früh-Green, G. L., Yoerger, D. R., Shank, T. M., Butterfield, D. A. & Hayes, J. M. (2005). A serpentinite-hosted ecosystem: the Lost City hydrothermal field. *Science* **307**, 1428–1434.

Kelley, K. A. & Cottrell, E. (2009). Water and the oxidation state of subduction zone magmas. *Science* **325**, 605–607.

Klein, F. & Bach, W. (2009). Fe–Ni–Co–O–S phase relations in peridotite–seawater interactions. *Journal of Petrology* **50**, 37–59.

Klein, F., Bach, W., Jöns, N., McCollom, T., Moskowitz, B. & Berquo, T. (2009). Iron partitioning and hydrogen generation

during serpentinization of abyssal peridotites from 15°N on the Mid-Atlantic Ridge. *Geochimica et Cosmochimica Acta* **73**, 6868–6893.

Kretz, R. (1983). Symbols for rock-forming minerals. *American Mineralogist* **68**, 277–279.

Johnson, J. W., Oelkers, E. H. & Helgeson, H. C. (1992). SUPCRT92: A software package for calculating the standard molal thermodynamic properties of minerals, gases, aqueous species, and reactions from 1 to 5000 bar and 0 to 1000°C. *Computers and Geosciences* **18**, 899–947.

Jolivet, L., Dubois, R., Fournier, M., Goffé, B., Michard, A. & Jourdan, C. (1990). Ductile extension in Alpine Corsica. *Geology* **18**, 1007–1010.

Lahondère, D. (1988). Le métamorphisme éclogitique dans les orthogneiss, et les métabasites ophiolitiques de la région de Farinole (Corse). *Bulletin de la Société Géologique de France* **4**, 579–585.

Lahondère, D. (1996). *Les schistes bleus et les éclogites à lawsonite des unités continentales et océaniques de la Corse alpine: nouvelles données pétrologiques et structurales. Documents du BRGM* **240**, 286 p.

Lee, C.-T. A., Luffi, P., Le Roux, V., Dasgupta, R., Albarède, F. & Leeman, W. (2010). The redox of arc mantle using Zn/Fe systematics. *Nature* **468**, 681–685.

Lemaire, C., Guyot, F. & Reynard, B. (1999). Vibrational spectroscopy (IR and Raman) of OH groups in chrysotile lizardite and antigorite. Presented at European Union of Geosciences 10, Strasbourg, 654 pp.

Malaspina, N., Poli, S. & Fumagalli, P. (2009). The oxidation state of metasomatized mantle wedge: insights from C–O–H-bearing garnet peridotite. *Journal of Petrology* **50**, 1533–1552.

Malavieille, J., Chemenda, A. & Larroque, C. (1998). Evolutionary model for Alpine Corsica: mechanism for ophiolite emplacement and exhumation of high-pressure rocks. *Terra Nova* **10**, 317–322.

Marcaillou, C., Muñoz, M., Vidal, O., Parra, T. & Harfouche, M. (2011). Mineralogical evidence for H_2 degassing during serpentinization at 300°C/300 bar. *Earth and Planetary Science Letters* **303**, 281–290.

Markl, G. (1999). Wollastonite formation during Variscan post-tectonic cooling in the Schwarzwald, Germany. *Mineralogy and Petrology* **66**, 193–213.

Massonne, H.-J. & Schreyer, W. (1987). Phengite geobarometry based on the limiting assemblage with K-feldspar, phlogopite, and quartz. *Contributions to Mineralogy and Petrology* **96**, 212–224.

Moody, J. (1976). Serpentinization: a review. *Lithos* **9**, 125–138.

Normand, C. & Williams-Jones, A. E. (2007). Physicochemical conditions and timing of rodingite formation: evidence from rodingite-hosted fluid inclusions in the JM Asbestos mine, Asbestos, Québec. *Geochemical Transactions* **8**, 1–19.

O'Brien, J. P. & Rodgers, K. A. (1973). Xonotlite and rodingites from Wairere, New Zealand. *Mineralogical Magazine* **39**, 233–240.

Parkinson, I. J. & Arculus, R. J. (1999). The redox state of subduction zones: insights from arc-peridotites. *Chemical Geology* **160**, 409–423.

Piccoli, G. C., Maletto, G., Bosio, P. & Lombardo, B. (2007). *Minerali del Piemonte e della Valle d'Aosta*, Alba (Cuneo): Associazione Amici del Museo 'F. Eusebio' Alba, 607 pp.

Ravna, E. J. K., Andersen, T. B., Jolivet, L. & De Capitani, C. (2010). Cold subduction and the formation of lawsonite eclogite—constraints from prograde evolution of eclogitized pillow lava from Corsica. *Journal of Metamorphic Geology* **28**, 381–395.

Rubie, D. C. (1986). The catalysis of mineral reactions by water and restrictions on the presence of aqueous fluid during metamorphism. *Mineralogical Magazine* **50**, 399–415.

Rüpke, L., Morgan, J. P., Hort, M. & Connolly, J. A. D. (2004). Serpentine and the subduction zone water cycle. *Earth and Planetary Science Letters* **223**, 17–34.

Seyfried, W. E., Foustoukos, D. I. & Fu, Q. (2007). Redox evolution and mass transfer during serpentinization: An experimental and theoretical study at 200°C, 500 bar with implications for ultramafic-hosted hydrothermal systems at mid-ocean ridges. *Geochimica et Cosmochimica Acta* **71**, 3872–3886.

Song, S., Su, L., Niu, Y., Lai, Y. & Zhang, L. (2009). CH_4 inclusions in orogenic harzburgite: Evidence for reduced slab fluids and implication for redox melting in mantle wedge. *Geochimica et Cosmochimica Acta* **73**, 1737–1754.

Stolper, E. & Newman, S. (1994). The role of water in the petrogenesis of Mariana trough magmas. *Earth and Planetary Science Letters* **121**, 293–325.

Trommsdorff, V. (1968). The wollastonite reaction in the western Bergell Alps. *Schweizerische Mineralogische und Petrographische Mitteilungen* **48**, 828–829.

Tsikouras, B., Karipi, S., Grammatikopoulos, T. A. & Hatzipanagiotou, K. (2006). Listwaenite evolution in the ophiolite mélange of Iti Mountain (continental Central Greece). *European Journal of Mineralogy* **18**, 243–255.

Vitale Brovarone, A., Beltrando, M., Malavieille, J., Giuntoli, F., Tondella, E., Groppo, C., Beyssac, O. & Compagnoni, R. (2011*a*). Inherited ocean–continent transition zones in deeply subducted terranes: Insights from Alpine Corsica. *Lithos* **124**, 273–290.

Vitale Brovarone, A., Groppo, C., Hetényi, G., Compagnoni, R. & Malavieille, J. (2011*b*). Coexistence of lawsonite-bearing eclogite and blueschist: phase equilibria modelling of Alpine Corsica metabasalts and petrological evolution of subducting slabs. *Journal of Metamorphic Geology* **29**, 583–600.

Wenk, H. R. (1969). Polymorphism of wollastonite. *Contributions to Mineralogy and Petrology* **22**, 238–247.